Available online at www.sciencedirect.com
SCIENCE DIRECT®
Journal of Catalysis 224 (2004) 80–93
JOURNAL OF CATALYSIS
www.elsevier.com/locate/jcat

On the mechanism of catalyzed isobutane/butene alkylation by zeolites

Andreas Feller, Alexander Guzman, Iker Zuazo, and Johannes A. Lercher *

Lehrstuhl II für Technische Chemie, Technische Universität München, Lichtenbergstrasse, 4, D-85747 Garching, Germany

Received 1 December 2003; revised 16 February 2004; accepted 17 February 2004

Abstract

Well-characterized examples of the large-pore zeolites X and Y in their acidic form were explored as catalysts for isobutane/butene alkylation in order to understand the principal requirements for successful solid acid catalysts. The materials were tested in a continuously operated stirred tank reactor under industrially relevant conditions. A high ratio of Brønsted to Lewis acid sites and a high concentration of strong Brønsted acid sites are seen to cause high hydride transfer activity and are mandatory for long catalyst life. Isobutane "self-alkylation" activity is higher in catalysts with a high hydride transfer activity. The catalyst lifetime is very sensitive with respect to the reaction temperature reaching the optimum between 70 and 80 °C concurrent with a maximum in self-alkylation activity. The lifetimes were found to be correlated linearly with the reciprocal of the olefin space velocity, while it hardly influenced the total productivity of the catalysts. The selectivities on the other hand strongly depended on the butene feed rate per active site.
© 2004 Elsevier Inc. All rights reserved.

Keywords: Heterogeneous catalysis; Alkylation; Zeolites; Acidity; Hydride transfer

1. Introduction

The importance of isobutane/butene alkylation in the refining industry as a source of a clean high-octane gasoline component is very high [1,2]. Industrial processes are currently based on sulfuric and hydrofluoric acid as catalysts with carbenium ions being the most important intermediates. Processes utilizing solid acid catalysts have not been successfully developed, because the rapid deactivation of the solid catalysts hindered the development of commercially attractive large-scale solutions. The countless efforts to overcome this problem are, however, well documented in the literature [3,4].

As Brønsted acid sites are needed to produce carbenium ions from olefins, a wide range of Brønsted acidic materials has been tested as solid alkylation catalysts. Among oxide-based materials, the noncorrosive, nontoxic, large-pore zeolites have the highest concentration of sufficiently strong Brønsted acid sites. Among the zeolites explored so far, materials based on the faujasite structure and zeolite BEA showed the best performance [3,4]. The catalyst productivity depends on the Brønsted acid site concentration (see Refs. [5,6]) which in turn is governed by the concentration of aluminum in the zeolite lattice. In this respect it is important to note that the maximum concentration of aluminum in the lattice is substantially lower for zeolite BEA than for faujasites.

Prior to this, a number of studies have been devoted to these materials. However, in many cases the experiments were conducted in fixed-bed or batch reactors under conditions of ill-defined catalyst activity and rapid catalyst deactivation. Thus, the correlation among the physicochemical properties of the material, the reaction conditions, and the catalytic properties has remained ambiguous. The strongly debated role of the strength and concentration of Brønsted and Lewis acid sites is an especially important example for that situation.

It has been proposed that only very strong Brønsted acid sites are active in alkylation [7], while other authors suggest that Brønsted sites with intermediate strength are catalytically active [8]. Agreement exists that very weak Brønsted acid sites only catalyze oligomerization [9]. Equally, the influence of Lewis acid sites, such as extraframework aluminum (EFAL) species, resulting from the (sometimes deliberate) dealumination of the zeolite framework is not fully understood. The presence of such sites could lead to an increase in the strength of some Brønsted acid sites, but might also neutralize Brønsted acid sites [10]. In addition, Lewis acid sites have been proposed to enhance the rate of deacti-

* Corresponding author. Fax: +49-89-28913544.
E-mail address: johannes.lercher@ch.tum.de (J.A. Lercher).

0021-9517/$ – see front matter © 2004 Elsevier Inc. All rights reserved.
doi:10.1016/j.jcat.2004.02.019

vation by catalyzing dehydrogenation leading to unsaturated carbenium ions [11] and by increasing the butene concentration close to the Brønsted acid sites [5].

The influence of important process parameters such as reaction temperature and olefin space velocity needs further examination. De Jong et al. [12] developed a basic kinetic model to describe the influence of the paraffin/olefin ratio and the olefin space velocity on the lifetime of selected catalysts. Extended catalyst lifetimes were achieved by using a continuous stirred tank reactor, which (assisted by low butene space velocities and high paraffin/olefin ratios) assured a low alkene concentration throughout the reactor. De Jong et al. reported oligomerization to be two orders of magnitude faster than hydride transfer, while Simpson et al. [13] using a plug-flow reactor with very dilute feed suggested even three orders of magnitude difference. This difference is attributed to the fact that hydride transfer is sterically more demanding than alkene addition. Taylor and Sherwood [14] developed an alternative kinetic model to estimate the lifetime of the catalyst dependent on several process parameters, including the reaction temperature. It was concluded that all changes in experimental conditions, which increase the concentration of unreacted alkenes, decrease the catalyst lifetime and product quality. The optimum reaction temperature was claimed to balance butene conversion and oligomerization activity.

In this work, a variety of modified acidic faujasites samples was examined to establish correlations among the physicochemical properties, the process conditions, and the alkylation mechanism on the other. These findings are related to the observations with zeolite BEA, which have been reported earlier (see, e.g., Refs. [5,31]).

2. Experimental

2.1. Material synthesis

The parent material for most of the materials prepared in this study was a Na-X faujasite with a bulk silicon/aluminum ratio (Si/Al) of 1.2. It was brought into the acidic form by aqueous exchange with 0.2 M lanthanum nitrate solution and in some experiments by additional aqueous exchange with ammonium nitrate solution in various concentrations. The liquid-to-solid ratios in these experiments were usually approximately 10 ml/g. The temperature during exchange was kept at 70 °C and the exchange time was 2 h. This procedure was typically repeated 2–3 times. After washing the resulting material with doubly distilled water until it was nitrate free and drying at 100 °C, the samples were calcined either in flowing air or under static air conditions with a slow temperature increment up to 450 °C. One sample was calcined in vacuum at 10^{-2} mbar. To further lower the sodium content of the zeolites, an additional ion-exchange step followed by washing, drying, and calcining was carried out.

To exclude biased conclusions based on low-quality starting materials, alternative Na-X parent materials and other La sources were also investigated, but the results were essentially identical to those reported here. For comparison, also a Na-Y (Si/Al = 2.5) was exchanged with La^{3+} and NH_4^+ ions and a Na-H-USY (Si/Al = 2.5, framework Si/Al ≈ 5), which was exchanged with NH_4^+ to give H-USY.

2.2. Catalyst characterization

The ion-exchanged materials were characterized by SEM, ^{29}Si NMR, and ^{27}Al NMR. AAS was used to determine the Si/Al ratio and the Na^+ concentration, usually expressed as the molar ratio of residual Na^+ per Al^{3+}. Nitrogen adsorption at 77 K was applied on several exemplary samples to estimate the micropore volume. Prior to adsorption, the samples were activated in vacuum at 400 °C for 10 h.

For measuring the acidity, two different kinds of adsorption/desorption experiments were carried out, i.e., TPD of ammonia in vacuum with a mass spectrometer as detector to estimate the total concentration of acid sites and sorption of pyridine monitored by IR spectroscopy (using a Bruker IFS-88 FT-IR spectrometer with a home-built vacuum cell). For the latter the sample was pressed into a self-supporting wafer, which was placed into a sorption cell, where it was activated in vacuum for 1 h at 450 °C. Then, the sample was cooled down to 100 °C and pyridine at a partial pressure of 10^{-2} mbar was introduced into the system. After saturation of all acid sites, the sample was outgassed for 1 h at 100 °C followed by a linear increase of 10 K/min to 450 °C and maintenance of that temperature for 1 h. Subsequently, the cell was cooled down again to 100 °C. Spectra of the sample were taken before adsorption of pyridine at 100 °C, after outgassing at 100 and 450 °C. From this set of spectra, the ratio of Brønsted (as evidenced by the band of pyridinium ions at 1540 cm^{-1}) to Lewis acid sites (the band of coordinately bound pyridine at 1450 cm^{-1}) was calculated for $T = 100$ °C (B/L_{100}) and $T = 450$ °C (B/L_{450}). Ratios of extinction coefficients were taken from Ref. [15].

2.3. Catalytic experiments

The alkylation of isobutane with 2-butene was performed in a stirred tank reactor (50 ml Hastelloy C-276 autoclave from Autoclave Engineers Co.) operated in continuous mode at a stirring speed of 1700 rpm. The liquefied gases were received from Messer with a purity of 99.95% (isobutane) and 99.5% (*cis*-2-butene). The sample (typically 4–5 g in powder form) was activated in situ within the alkylation reactor at 170 °C for 16 h in flowing nitrogen. After cooling down to the reaction temperature, typically 75 °C, the reactor was filled with liquid isobutane at a pressure of 32 bar. The reaction was started by admitting a butene–isobutane mixture with a paraffin-to-olefin (P/O) ratio of 6.7 and a olefin space velocity (OSV) of 0.2 $g_{butene}/(g_{catalyst}\,h)$. In order to investigate the influence of the reaction temperature on

the alkylation mechanism, a study was performed on an exemplary catalyst at temperatures varying from 40 to 130 °C. On the same catalyst also the influence of the OSV was examined, varying this parameter from 0.17 to 0.80 h^{-1} with a paraffin-to-olefin ratio of 6.7. These conditions (with the exception of the temperature) are in the range at which the commercial processes typically operate.

The product left the reactor through a filter, which kept the catalyst particles in the suspension. Then, the product was expanded and passed through a six-port valve with a sample loop, the contents of which were injected automatically into an HP 6830 gas chromatograph equipped with a FID detector and a 35-m DB-1 column. Downstream of the six-port valve, the product stream was condensed into a cold trap cooled with a dry ice/isopropanol mixture (at −80 °C). The product was collected over the whole time on stream and was weighed and analyzed chromatographically to give the integral product composition. The results were compared with the mathematical integration of the differential data points gathered during the run, with the differences being less than 10%.

To measure the true alkylation performance of the catalysts, the butene conversion must be complete (which also is the industrial mode of operation). When operating at low conversion levels, oligomerization predominates with mainly unsaturated products and rapid catalyst deactivation. Note that the alkylation reaction is not performed in steady state. When the reaction is started, the reactor contains only isobutane. With the introduction of the isobutane/butene mixture and the subsequent (near-) complete conversion of butene, the reactor content steadily changes its composition to an isobutane/products mixture, with an increasing fraction of products. Under typical conditions (catalyst mass = 5 g, P/O ratio = 6.7, and OSV = 0.2 h^{-1}), steady state is theoretically reached after approx 20 h, with the exit stream consisting of a 20–25 wt% products in isobutane mixture. However, typical catalyst lifetimes were in the range of 5 to 12 h. Hence, steady-state conditions were not reached. With the knowledge of the theoretical butene build up curve derived from the mass balance (and its experimental verification in a blank run without catalyst) conversions and yields were calculated. At complete butene conversion the theoretical maximum yield is 2.04 $g_{product}/g_{butene}$, assuming a 1/1 stoichiometry of isobutane alkylation with butene.

3. Results

3.1. Physicochemical characterization

About 20 different samples were prepared via La^{3+} and NH_4^+ exchange steps followed by calcination in flowing or static air. With two calcination steps zeolite X was brought to a Na^+ level lower than 0.5%. Using only one calcination step, but performing multiple ammonium-exchange steps, resulted in a poorer exchange level. The benefit of employing a repeated exchange-calcination procedure has been described earlier [16]. The author reported that zeolite X was easier to exchange than zeolite Y. The same was observed here; i.e., lower exchange levels were achieved with zeolite Y compared to zeolite X.

Micropore volumes of the La-X samples were of the order of 0.16 ml/g, the La-Y samples exhibited similar pore volumes, and the H-USY sample showed a micropore volume of 0.15 ml/g.

Pyridine sorption experiments revealed that zeolite X has a significantly higher fraction of strong Brønsted acid sites than zeolite Y. This leads to comparable B/L_{100}, but to considerably different B/L_{450} values, which are much higher for the X samples. Next to the bands at 1540 and 1450 cm^{-1}, also a band at ca. 1445 cm^{-1} was detected. This band has been attributed to Na^+ or La^{3+} cations, which both act as weak Lewis acid sites, as concluded from the complete desorption of pyridine from these sites at 450 °C. Fig. 1 displays a typical spectrum of a La-X sample before and after pyridine adsorption at 100 °C and after desorption at 450 °C (measured after cooling to 100 °C). In the hydroxyl region four bands were observed, i.e., (i) the silanol band at 3740 cm^{-1}, (ii) the band at 3637 cm^{-1} (acidic hydroxyl group), (iii) the band at 3596 cm^{-1} (acidic hydroxyl group), and the band characteristic for the nonacidic lanthanum hydroxyl group at 3512 cm^{-1}. Upon adsorption of pyridine, the acidic hydroxyl bands at 3637 and 3596 cm^{-1} disappeared. The silanol band at 3740 cm^{-1} did not disappear completely and the La–OH group did not interact with pyridine. After desorption to 450 °C the weakly acidic SiOH band and the band at 3637 cm^{-1} reappeared completely, while a substantial fraction of the hydroxyls characterized by the band at 3596 cm^{-1} retained pyridine.

The overall acid site concentration as measured with NH_3-TPD was between 0.6 and 0.8 mmol/g for all the La-X samples. The values for the Y zeolites were slightly higher, around 1 mmol/g.

SEM was used to analyze the crystal size. The zeolite X samples showed an average crystal size between 1 and 2 μm, the zeolite Y samples between 0.5 and 1 μm.

^{27}Al MAS-NMR discerned for all the measured samples three different aluminum species. Besides the signal at approx 50–60 ppm representing tetrahedrally coordinated Al, and the signal at 0 ppm for octahedral Al, also a broad signal between 40 and 10 ppm was detected. For the La-X samples, this was the most prominent signal, accounting for about 70% of the total signal area. The assignment of this signal is not straightforward. It has been reported to represent distorted tetrahedral framework Al in both La-free [17] and La-containing [18,19] samples, but it could also indicate a second type of poorly ordered extraframework Al [20] and pentacoordinated Al [19]. ^{29}Si MAS-NMR was used on several La-X samples and the parent Na-X. The Si(nAl) signals (n represents the number of aluminum atoms in the second coordination sphere of the silicon atom) with the La-X samples were high-field-shifted compared to the

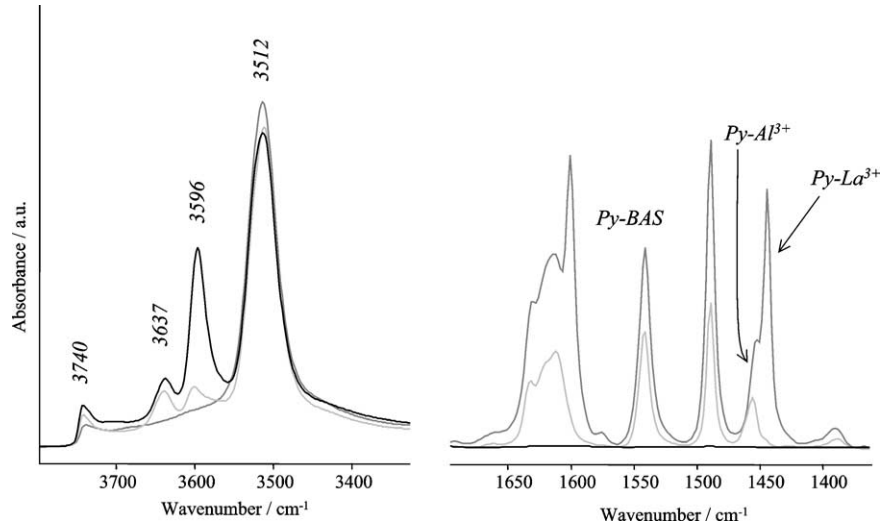

Fig. 1. IR spectra of La-X sample after activation at 450 °C (black line); sample with pyridine adsorbed at 100 °C (dark gray line); sample after degassing at 450 °C (light gray line). All spectra were taken at 100 °C.

signals in Na-X. In La-X the chemical shifts were −88.9, −93.1, −96.7, −102.1, and −105.5 ppm for Si(nAl) atoms with $n = 4$, 3, 2, 1, and 0, respectively. The corresponding chemical shifts for Na-X were −84.0, −88.4, −93.6, −98.4, and −102.1 ppm. This upward shift is attributed to a local strain of framework SiO_4 tetrahedra caused by neighboring large La cations [18]. Si/Al ratios were calculated from the signal areas. For the parent Na-X the Si/Al ratio was determined to be 1.18, which is in good agreement with the elemental analysis. The La-X samples had Si/Al ratios between 1.10 and 1.28. Although these values seemed rather low compared to the sodium form, they increased with decreasing B/L ratio reflecting the increasing degree of dealumination. The Si/Al ratios of the La-containing materials may be underestimated due to an overlap of the La-distorted Si(4Al) signal (−88.9 ppm) with the nondistorted Si(3Al) signal (−88.4 ppm) as was suggested by Gaare and Akporiaye for La exchanged X and Y zeolites [21].

3.2. Activity and selectivity in alkylation of isobutane with n-butene

The alkylation reaction was performed with every exchanged sample, employing a reaction temperature of 75 °C, an olefin space velocity of 0.2 $g_{butene}/(g_{catalyst}\,h)$, and a P/O ratio of 6.7. The lifetimes achieved varied from 3 to 12 h.

Before we describe the differences among the tested materials, a typical case is described in detail. Fig. 2 compiles the conversion (a) and the yield (b) of a representative La-X sample. The lifetime, defined as the time of the (near-) complete butene conversion, was approximately 11 h. Then, the conversion sharply dropped to values below 60%. The yield steadily increased for the first 5 h TOS, reaching the theoretical maximum and staying nearly constant for the next 5 h. With the decrease in conversion, also the yield decreased to values below 1 g/g. The slow increase in yield for the first hours on stream is attributed to a build up of hydrocarbons in the catalyst pores, especially on the acid sites. The integrated area between the curve and the theoretical maximum amounts to an average 2.3–2.7 butene molecules per acid site suggesting addition between one and two butene molecules to the alkoxy group.

Fig. 3a displays the selectivities to the three main product fractions, i.e., the hydrocarbons with 5 to 7 carbon atoms, the octane fraction, and the fraction with 9 and more carbon atoms as a function of time on stream. Additionally, the selectivity to n-butane is shown, which was produced in substantial amounts in the beginning. The main products were isooctanes with an initial selectivity of 85 wt%, which decreased with time on stream to a value of approximately 60 wt%. The selectivity to the cracked products (C_5–C_7) passed through a maximum of approximately 18 wt% at 9 h TOS. The heavy alkylation products (C_{9+}) had a constant low selectivity during the first 5 h, after which the selectivity increased to values above 30 wt%. The n-butane selectivity monotonously declined from a start value of approximately 8 wt%.

The selectivity in the C_8 region is shown in Fig. 3b. The main components were the trimethylpentanes 2,2,4-TMP, 2,3,3-TMP, and 2,3,4-TMP, which made up together more than 80 wt% of the total C_8 fraction. The characteristic increase in 2,2,4-TMP selectivity during the first hours TOS and the subsequent decline was seen with all La-containing samples of zeolite X. The fourth TMP, 2,2,3-TMP, which is the primary product of the alkylation of isobutane with 2-butene, could not be separated from 2,5-DMH. Their combined selectivity showed the same TOS behavior as 2,2,4-TMP, with values between 7 and 14 wt% of the C_8 fraction. The others, 2,3-DMH, 2,5-DMH, and 3,4-DMH had selectivities below 5 wt% during the time of complete butene conversion. When the conversion started to drop, the selectivity to 3,4-DMH increased and octenes were

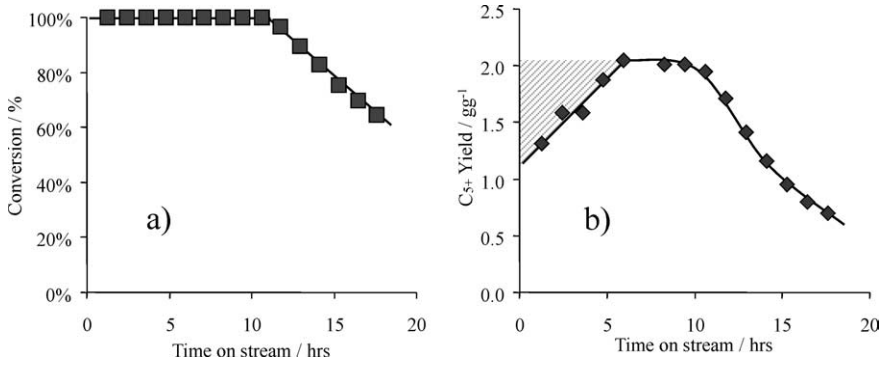

Fig. 2. Alkylation performance of a typical La-X catalyst. (a) Butene conversion as a function of time on stream; (b) C_{5+} product yield as a function of time on stream. $T = 75\,^{\circ}\mathrm{C}$, OSV $= 0.18\ \mathrm{h}^{-1}$, P/O ratio $= 6.7$. The shaded area represents the buildup of hydrocarbons on the zeolite surface.

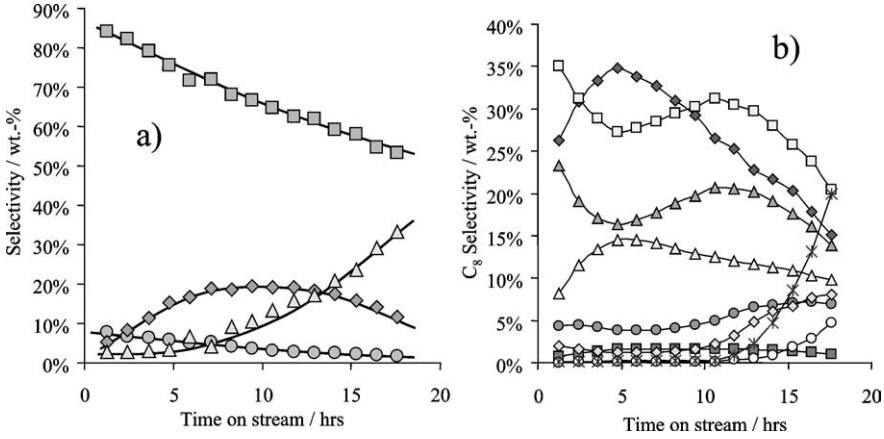

Fig. 3. Alkylation performance of a typical La-X catalyst. (a) Product group selectivities with time on stream (●, *n*-butane; ◆, C_5–C_7 products; ■, C_8 products; △, C_{9+} products); (b) selectivities in the C_8 fraction with time on stream (◆, 2,2,4-TMP; ■, 2,4-DMH; △, 2,5-DMH/2,2,3-TMP; ▲, 2,3,4-TMP; □, 2,3,3-TMP; ●, 2,3-DMH; ○, 4-MHp/3,4-DMH; ◇, 3,4-DMH; ⋆, octenes). $T = 75\,^{\circ}\mathrm{C}$, OSV $= 0.18\ \mathrm{h}^{-1}$, P/O ratio $= 6.7$.

observed in the product stream. Then, the octenes rapidly became the dominant product, indicating a switch in the reaction from alkylation to dimerization.

The results compiled in Figs. 2 and 3 clearly demonstrate the problems associated with the use of a tubular/plug-flow reactor. Using a plug-flow reactor, a marked concentration gradient in alkenes and products exists over the length of the catalyst bed, so that at a certain time on stream catalyst particles at different positions in the bed will catalyze different reactions. Consequently, the product at the reactor exit will be a mixture of products of different deactivation stages and the catalyst particles at the top of the active zone will experience a much higher alkene concentration than the particles in a backmixed reactor under identical macroscopic operating conditions. In consequence, this will lead to a more rapid decrease in the lifetime of the catalyst particles at the top of the active catalyst bed. After some time on stream, these deactivated catalyst particles will produce octenes, which will subsequently react further downstream in a zone containing still fully active sites producing heavy alkylation products. These will either desorb as such or undergo further cracking. With the continuously operated stirred tank reactor, ideally, all particles are in contact with the same fluid at the same time on stream. Therefore, all particles show the same state of deactivation and experience a much lower severity with respect to the alkene concentration. Furthermore, the product from a CSTR will contain much more of the primary products, the trimethylpentanes, while with a PFR generally more oligomerization/cracking products are formed. To produce high-quality alkylate in a plug-flow reactor very high P/O ratios and low OSV must be used. Note that it is possible in this way to slow down the deactivation process, but not to prevent the coexistence of catalyst particles with a broad distribution of deactivation states.

Thus, the CSTR allows for a more detailed data analysis, when examining the total amount of individual compounds produced with TOS. In Fig. 4a this is shown for the different product groups; Fig. 4b displays the total production of individual octanes (normalized against the catalyst mass) with TOS. The dashed line represents the end of the catalyst lifetime. As can be seen, the production of the trimethylpentanes was nearly constant over the catalyst lifetime with a sudden stop when the catalyst deactivates. The cracking activity also ceased completely at this point. The only compounds, which were produced after the conversion started dropping, were 3,4-DMH, octenes, and some of the heavier hydrocarbons. Whether these compounds are alkanes or alkenes is unclear at this point. It is noteworthy that the production of

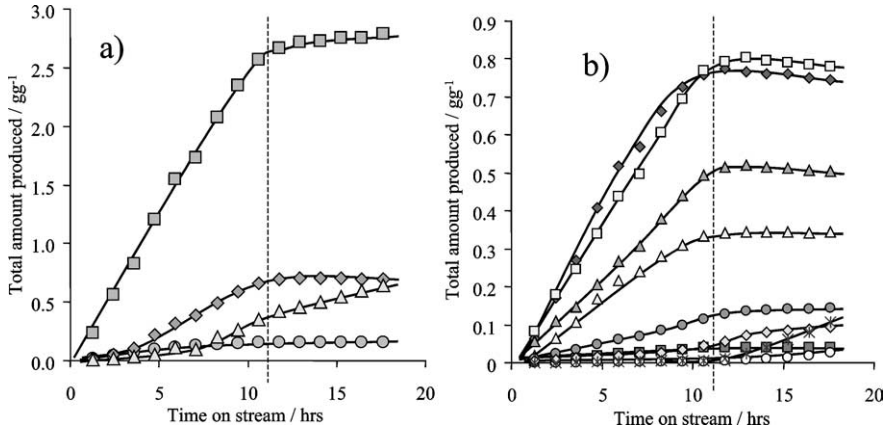

Fig. 4. Alkylation performance of a typical La-X catalyst. (a) Total amount produced of the different product groups with time on stream (●, *n*-butane; ◇, C_5–C_7 products; ■, C_8 products; △, C_{9+} products); (b) total amounts produced of the individual C_8 products with time on stream (◇, 2,2,4-TMP; ■, 2,4-DMH; △, 2,5-DMH/2,2,3-TMP; ▲, 2,3,4-TMP; □, 2,3,3-TMP; ●, 2,3-DMH; ○, 4-MHp/3,4-DMH; ◇, 3,4-DMH; ⋆, octenes). $T = 75\,^{\circ}C$, P/O ratio = 6.7, OSV = 0.18 h^{-1}. The dashed line represents the end of the lifetime of the catalyst.

n-butane slowed down some hours earlier than that of the other products. The slight decrease in the produced mass of the trimethylpentanes during the last stage of the reaction suggests that these alkane molecules are consumed under these reaction conditions with a small rate.

3.3. Influence of the acidity

After the detailed description of a typical case, the relationship between the acidity of the individual catalyst samples and their performance in the alkylation is addressed. All examined materials were active and selective alkylation catalysts. In general, zeolite X samples showed longer lifetimes than zeolite Y samples.

The acidity of zeolites has extensive and intensive components. The IR spectra of sorbed pyridine allow estimating the concentration of Brønsted and Lewis acid sites and their relative strength. From this, the ratios of Brønsted to Lewis acid sites at specific (outgassing) temperatures representing different strengths of the acid sites can be estimated. A strong correlation between the Brønsted/Lewis ratios measured at 450 °C was found. With increasing ratios of Brønsted to Lewis acid sites, the catalyst lifetimes increased. The correlation is directly proportional to the fraction of strong Brønsted acid sites (as measured at 450 °C) among all strong acid sites (B/(B + L) ratio; see Fig. 5a). Interestingly, the total concentration of Brønsted or Lewis acid sites did not show a correlation with the catalyst lifetimes. A good correlation, however, was found for the concentration of strong Brønsted acid sites (Fig. 5b). The concentration of strong Lewis acid sites alone did not directly influence the alkylation performance.

Samples with varying lifetimes also showed varying selectivities. As these samples pass through different stages of deactivation at different absolute times on stream, the integral selectivities of alkylate produced until the end of the catalyst lifetime are used in this study. Note that this differs markedly from the practice in other reports, where

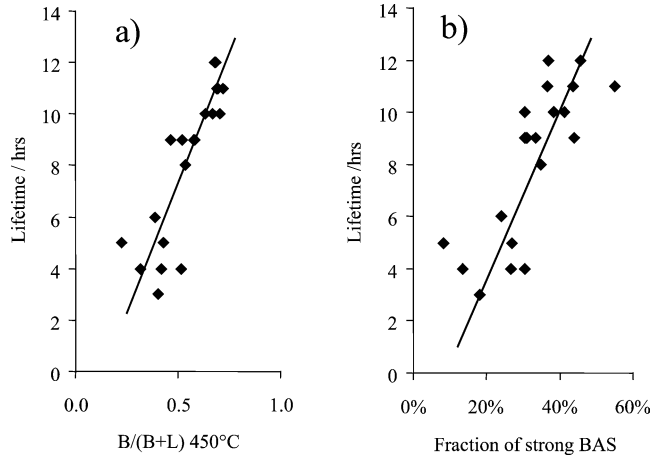

Fig. 5. Details of the acidity–lifetime correlations. (a) Catalytic lifetimes of the individual samples as a function of the Brønsted/(Brønsted + Lewis) acid site ratio measured at 450 °C; (b) catalytic lifetimes as a function of the fraction of strong Brønsted acid centers. All catalytic measurements were performed at $T = 75\,^{\circ}C$, OSV = 0.18 h^{-1}, P/O ratio = 6.7.

either data at very short TOS are compared or even selectivities at a later time-on-stream with varying conversion levels. The products compared are virtually free of alkenes and represent the yield along the usable lifetime. In Fig. 6a, the dependence of the integral selectivities to the different product groups on the lifetimes is shown. Each data point represents one individual alkylation experiment. For all samples, the isooctane fraction dominated the products. With increasing lifetime the C_8 selectivity increased from 60 to 75 wt% and slightly decreased again with catalysts of long lifetimes. The selectivity to cracking was independent of the lifetime with about 17 wt%. Most importantly, a steep decline in the selectivity to the heavy end products was seen with increasing lifetime from 20 down to 8 wt%. The selectivity to *n*-butane increased linearly with the lifetime from 1.6 wt% to nearly three times as much, 4.7 wt%. Note that the total amount of *n*-butane produced with the long living

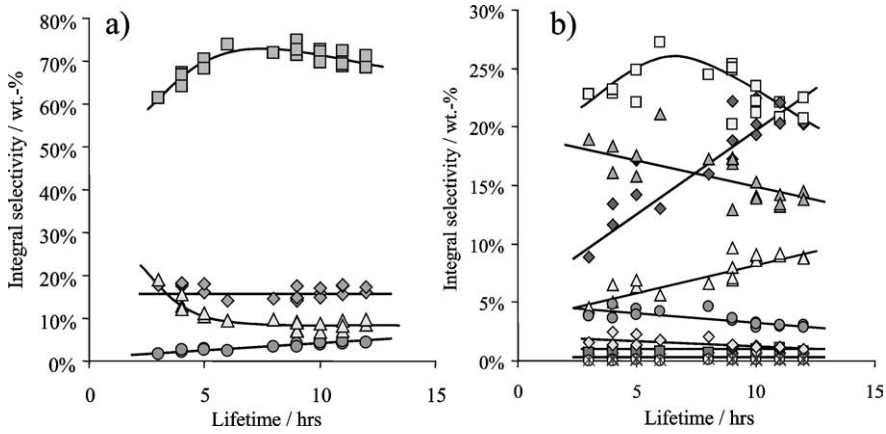

Fig. 6. Changes in selectivities with the lifetimes of the individual samples. (a) Integral selectivities to the different product groups as a function of the lifetimes of the individual samples (●, *n*-butane; ◆, C_5–C_7 products; ■, C_8 products; △, C_{9+} products); (b) integral selectivities to the individual C_8 products as a function of the lifetimes of the individual samples (◆, 2,2,4-TMP; ■, 2,4-DMH; △, 2,5-DMH/2,2,3-TMP; ▲, 2,3,4-TMP; □, 2,3,3-TMP; ●, 2,3-DMH; ○, 4-MHp/3,4-DMH; ◇, 3,4-DMH; ⋆, octenes). Each data point represents a single experiment. $T = 75\,^{\circ}\mathrm{C}$, OSV $= 0.18\ \mathrm{h}^{-1}$, P/O ratio $= 6.7$.

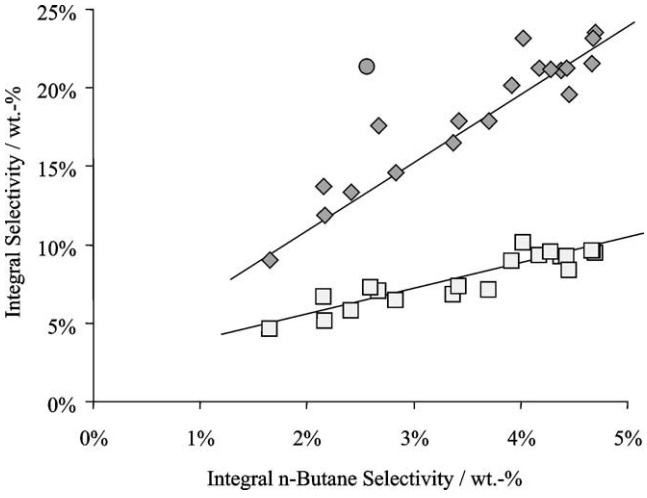

Fig. 7. The integral selectivities to 2,2,4-TMP (◆) and 2,5-DMH/2,2,3-TMP (□) as a function of the integral *n*-butane selectivity. The round symbol (●) represents the 2,2,4-TMP selectivity measured with H-USY. $T = 75\,^{\circ}\mathrm{C}$, OSV $= 0.18\ \mathrm{h}^{-1}$, P/O ratio $= 6.7$.

catalysts was more than four times higher than the number of acid sites in the sample.

Fig. 6b displays the integral selectivities in the C_8 fraction (not included: H-USY, see below). But unlike Fig. 3b, the selectivity is based on the total product and not on the C_8 fraction alone. This representation was used here, as it shows the relative rates of production for the individual compounds. With increasing lifetime, only the rates for 2,2,4-TMP and 2,2,3-TMP + 2,5-DMH increased steadily, while 2,3,3-TMP exhibited a maximum at intermediate lifetimes. The selectivities to the other products either decreased or did not change significantly. Thus, 2,2,4-TMP and 2,2,3-TMP + 2,5-DMH are concluded to be at large responsible for the increase in selectivity to the octane fraction as shown in Fig. 6a.

Fig. 7 demonstrates the linear interdependence among *n*-butane and 2,2,4-TMP and 2,2,3-TMP + 2,5-DMH. H-USY deviated from this trend (marked in Fig. 7 with the circular symbol). Here, the 2,2,4-TMP selectivity was higher than expected from the general trend, whereas the *n*-butane and 2,2,3-TMP + 2,5-DMH selectivity did not diverge.

3.4. Influence of the reaction temperature

One typical La-X catalyst (achieving 9 h lifetime at 75 °C) was used to explore the influence of the reaction temperature. The temperature was varied from 40 to 130 °C, keeping the other conditions (P/O ratio = 6.7, OSV = 0.2 $g_{butene}/(g_{catalyst}\,h)$) constant. Fig. 8 displays the lifetime dependent on the reaction temperature. The curve exhibits a surprisingly sharp maximum at 75 °C. A difference of only 35 °C downward and 55 °C upward was sufficient to reduce the lifetime to a fourth.

Also the selectivities changed drastically with the temperature, as can be seen in Fig. 9. The selectivities are presented in the same manner as in Fig. 6. Fig. 9a shows the decline in the isooctane selectivity with rising temperature, which was compensated by an increase in the cracking selectivity and at high temperatures also in the C_{9+} selectivity. The selectiv-

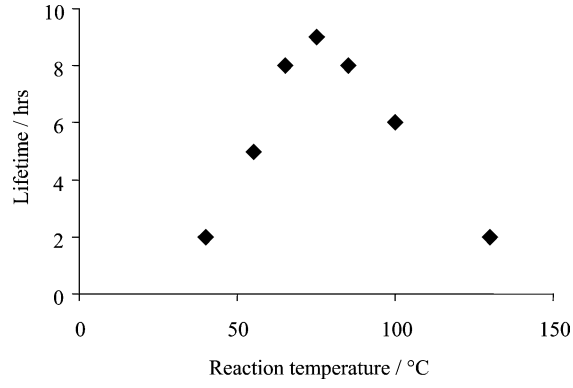

Fig. 8. Lifetime of La-X catalyst as a function of the reaction temperature. OSV $= 0.18\ \mathrm{h}^{-1}$, P/O ratio $= 6.7$.

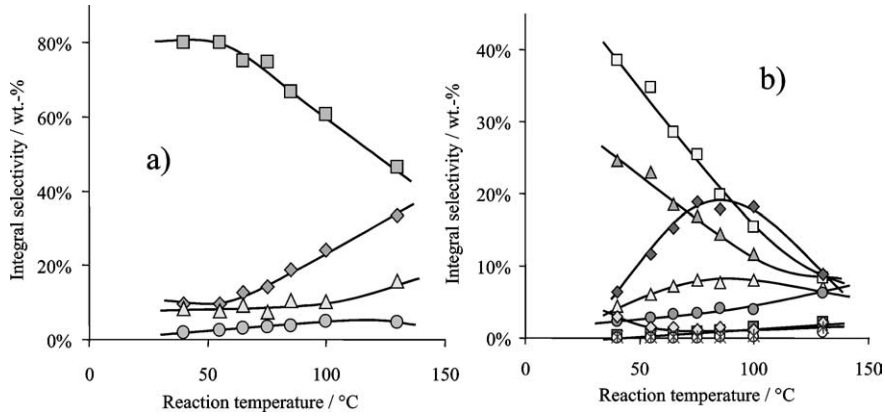

Fig. 9. Changes in selectivities as a function of the reaction temperature. Integral selectivities to the different product groups vs reaction temperature (●, *n*-butane; ◆, C_5–C_7 products; ■, C_8 products; △, C_{9+} products); (b) integral selectivities to the individual C_8 products vs reaction temperature (◆, 2,2,4-TMP; ■, 2,4-DMH; △, 2,5-DMH/2,2,3-TMP; ▲, 2,3,4-TMP; □, 2,3,3-TMP; ●, 2,3-DMH; ○, 4-MHp/3,4-DMH; ◇, 3,4-DMH; ⋆, octenes). OSV = 0.18 h^{-1}, P/O ratio = 6.7.

ity to *n*-butane increased by a factor of 3 to about 5 wt% and then slightly dropped again. Fig. 9b shows that the drastic decline in C_8 selectivity was caused by a steadily decreasing 2,3,4-TMP and 2,3,3-TMP selectivity, which was partly compensated by an increase in the 2,2,4-TMP selectivity. The 2,2,4-TMP and the 2,2,3-TMP + 2,5-DMH selectivity passed a maximum between 75 and 100 °C. The production of all dimethylhexanes increased with the reaction temperature.

3.5. Influence of olefin space velocity

The same catalyst, which was used for studying the influence of varying temperatures, was also used in a study on the influence of the OSV. The OSV was raised from 0.17 to 0.38 h^{-1} and 0.79 h^{-1} using a P/O ratio of 6.7. The lifetime was found to be linear with the reciprocal of the OSV (see Fig. 10a). In other words, the integral yields did not change significantly with varying space velocity. The same amount of alkylate was produced in shorter time. Increasing $(OSV)^{-1}$ lead to a slight increase in the *n*-butane selectivity and a concomitant slight decrease in the C_{9+} selectivity, as shown in Fig. 10b. Within the C_8 products, the selectivities to 2,2,4-TMP and 2,2,3-TMP + 2,5-DMH increased, while all other octane selectivities decreased (Fig. 10c).

3.6. Reactions with partly deactivated catalyst

The influence of already deactivated catalyst particles in a still active surrounding was examined in a series of experiments employing the same La-X sample as in the aforementioned series of experiments. For this, fresh catalyst was mixed with a fraction of deactivated catalyst. This mixture was activated as usual in the reactor and tested under

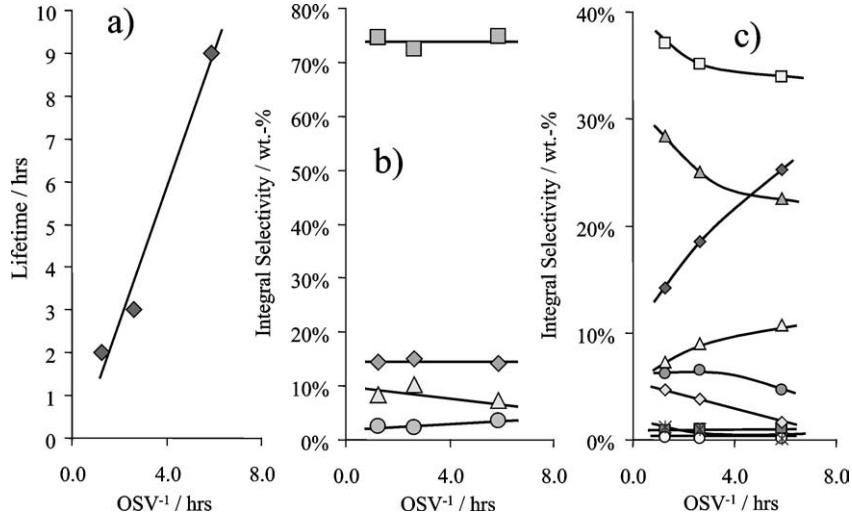

Fig. 10. Influence of the reciprocal of the olefin space velocity on the alkylation performance. (a) Lifetime vs $(OSV)^{-1}$; (b) integral product group selectivities as a function of $(OSV)^{-1}$ (●, *n*-butane; ◆, C_5–C_7 products; ■, C_8 products; △, C_{9+} products); (c) integral selectivities to the individual octanes as a function of $(OSV)^{-1}$ (◆, 2,2,4-TMP; ■, 2,4-DMH; △, 2,5-DMH/2,2,3-TMP; ▲, 2,3,4-TMP; □, 2,3,3-TMP; ●, 2,3-DMH; ○, 4-MHp/3,4-DMH; ◇, 3,4-DMH; ⋆, octenes). T = 75 °C, P/O ratio = 6.7.

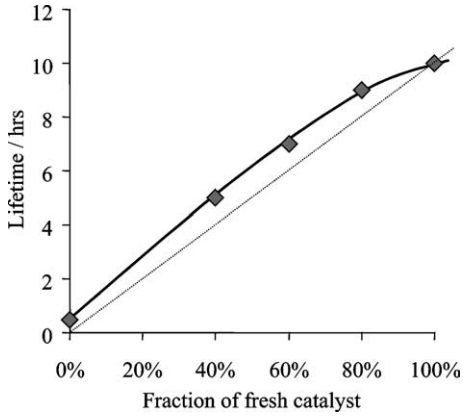

Fig. 11. Lifetime of a La-X sample with different amounts of added deactivated catalyst as a function of the fraction of fresh catalyst. $T = 75\,^{\circ}\mathrm{C}$, $\mathrm{OSV} = 0.18\ \mathrm{h}^{-1}$, P/O ratio = 6.7. The dotted line represents the theoretical linear behavior.

the standard conditions, i.e., $T = 75\,^{\circ}\mathrm{C}$, $\mathrm{OSV} = 0.18\ \mathrm{h}^{-1}$, and P/O ratio = 6.7. Mixtures with 20, 40, 60, and 100 wt% of deactivated catalyst were tested. The lifetimes as a function of the fraction of the fresh catalyst in the mixture are shown in Fig. 11. Assuming the already deactivated fraction to be completely inert, the remaining active part simply experiences a higher space velocity. The accordingly calculated lifetimes are represented by the dotted line in Fig. 11. The measured results exceeded the calculated lifetimes by 0.5–1 h. Even fully deactivated catalyst shows after the in situ activation a certain—although low—activity. The integral selectivities dependent on the fraction of fresh catalyst are depicted in Fig. 12. It can be seen that relatively more heavy end products were produced with decreasing amounts of fresh catalyst, whereas the production of cracked products and *n*-butane slightly decreased. The C_8 selectivity passed through a flat maximum. Within the C_8 fraction, the selectivity to 2,2,4-TMP strongly increased from ca. 7 wt% to ca. 23 wt%. The selectivity to 2,2,3-TMP + 2,5-DMH also increased with increasing fraction of fresh catalyst. When increasing the amount of deactivated catalyst from 60 to 100% drastic increases in heavy end, DMH, and octene selectivities were seen.

4. Discussion

4.1. Reactions influencing the product distribution

Fig. 13 displays the basic alkylation mechanism as adapted from Schmerling [22,23]. The product distribution is governed by the relative rates of the three individual steps, i.e., alkene addition, isomerization, and hydride transfer. The antagonistic pair of reactions, i.e., alkene addition–hydride transfer, determines the selectivity to single and multiple alkylation.

A high ratio of hydride transfer vs alkene addition retards the buildup of long hydrocarbon chains, which finally block the acid sites. Alkene addition is a much more facile reaction than hydride transfer. A high ratio of hydride transfer vs alkene addition can be achieved by employing a high P/O ratio in the feed, a high back mixing in the reactor (using CSTR-type reactors), by ensuring a low diffusion hindrance of the products out of the pores and by maximizing the hydride transfer rate as such.

The reaction pair isomerization–hydride transfer determines the preference for primary or equilibrium products. A fast hydride transfer shortens the time for isomerization of the adsorbed carbocations through hydride and methyl shifts, in this way reducing the formation of thermodynamically favored products. 2,2,3-TMP is the primary product of alkylation with 2-butene. In all experiments presented here, the integral selectivity was quite low, never exceeding 10 wt%. Speculatively, this is attributed to the steric difficulties to achieve hydride transfer, as the carbenium ion is protected by an isobutyl and an ethyl group, while all other TMP isomers have one methyl group adjacent to the carbon that forms the alkoxy bond to the catalyst.

Cracking through β-scission accounts for the C_5–C_7 products and the products with carbon atom numbers, which

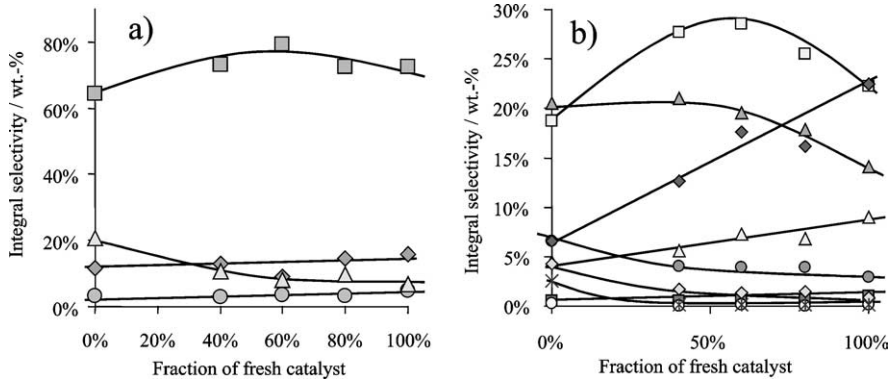

Fig. 12. Alkylation performance with different amounts of added deactivated catalyst. (a) Product group selectivities as a function of the fraction of fresh catalyst (●, *n*-butane; ◆, C_5–C_7 products; ■, C_8 products; △, C_{9+} products); (b) selectivities within the C_8 fraction as a function of the fraction of fresh catalyst (◆, 2,2,4-TMP; ■, 2,4-DMH; △, 2,5-DMH/2,2,3-TMP; ▲, 2,3,4-TMP; □, 2,3,3-TMP; ●, 2,3-DMH; ○, 4-MHp/3,4-DMH; ◇, 3,4-DMH; ×, octenes). $\mathrm{OSV} = 0.18\ \mathrm{h}^{-1}$, P/O ratio = 6.7, $T = 75\,^{\circ}\mathrm{C}$.

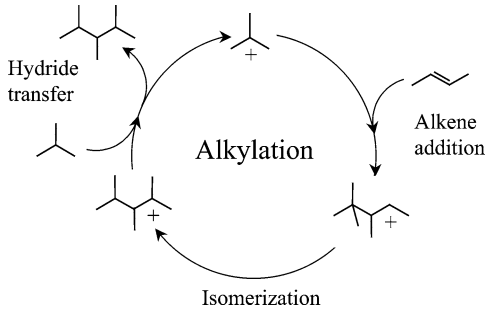

Fig. 13. Simplified alkylation cycle including the three key reaction steps.

are not multiples of four. Cracking is concluded to occur on the same acid sites as alkylation. Olefinic fragments from cracking are found only in traces. As long as the catalyst is active olefins are added to the carbenium ions and are quantitatively removed. Therefore, cracking of a C_{12} carbenium ion leads to one C_5–C_7 carbenium ion (alkoxy group) and one corresponding alkene that will be added to another carbenium ion. Both can desorb via hydride transfer from isobutane as alkanes. Cracking most likely also accounts for some of the produced octanes. However, for the experiments at 75 °C, a correlation between individual octane selectivities and cracking selectivity (which was scattered over a narrow range of 12–18 wt%) could not be established.

Weak Brønsted acid sites catalyze dimerization [24]. The more demanding reactions cracking and hydride transfer do not proceed on these sites. Therefore, octenes are produced that adsorb or react with alkoxy groups and so enhance the rate of deactivation. Consequently, the lower the concentration of weak acid sites, the higher the relative contribution of hydride transfer rate (on alkoxy groups on the strong Brønsted acid sites) will be and the longer the catalyst will be active. This is reflected in the correlation between the fraction of strong Brønsted acid sites and the lifetime of the catalyst shown in Fig. 5b.

4.2. Reactions leading to heavy end products

After a significant time of constant activity, the hydride transfer activity stopped surprisingly abrupt, as shown in Fig. 4. Most saturated compounds (with the exception of 3,4-DMH) ceased being produced at this point. This suggests a parallel progress of the deactivation with respect to all active sites in the reactor, a feature which is unique for CSTR-type reactors. On the individual site, this means that the hydride transfer comes to a sudden stop, rather than slowing down. The cracking activity stops also simultaneously. Oligomerization (including dimerization) is the only reaction proceeding. This confirms the existence of two different active sites in zeolites during alkylation, i.e., strong sites catalyzing (multiple) alkylation and cracking and weak sites catalyzing oligomerization. The C_{9+} products originate from multiple alkylation on the stronger sites and oligomerization on the weaker sites. When the strong sites are deactivated, multiple alkylation ceases, while oligomerization on the weaker sites still proceeds. This is reflected in the changing slope of the C_{9+} curve in Fig. 4. The sudden deactivation can be caused either by site blocking of the true alkylation sites or by pore blocking. The present data do not suffice to attribute the deactivation behavior unequivocally to one of the reasons. However, the latter (pore blocking) would imply that an important fraction of the oligomerization sites is located on the outer surface of the zeolite particles.

4.3. Self-alkylation and its importance for alkylation

Following the most basic reaction scheme, the reactor contains only isobutane at the beginning of the reaction. With the introduction of the isobutane/2-butene mixture, 2-butene adsorbs on the Brønsted sites and forms secondary butoxy groups. To these 2-butene can be added forming a 3,4-dimethylhexyloxy group, which desorbs via hydride transfer as a DMH, leaving a tertiary butoxy group on the acid site. Fig. 3 shows that this occurs to some extent, because the initial 3,4-DMH selectivity is slightly higher than after a few hours TOS. The sec.-butoxy group can also directly undergo a hydride transfer. This will free *n*-butane and leave a tertiary butoxy group. As *n*-butane is not a primary product of β-scission of an alkoxy group, the only way of producing it is this initiating reaction step. Assuming that butenes do not desorb from the acid sites, this can only happen once per acid site. Consequently, the total amount of *n*-butane produced should not exceed the number of acid sites. Surprisingly, with the long-living samples, more than four times the amount of *n*-butane was found. The most straightforward mechanism to account for the pronounced formation of *n*-butane is the decomposition of the isobutoxy group into isobutene and a free Brønsted acid site. This reaction sequence has been denoted as a part of the self-alkylation cycle [13,25–27]. Self-alkylation is of importance in hydrofluoric acid-catalyzed processes [4]. The importance of this mechanism depends on the feed alkene and the reaction temperature. Its importance was found to increase with the molecular weight and increased branching of the feed alkene [28]. Generally, sulfuric acid is less active for self-alkylation than hydrofluoric acid. The corresponding catalytic cycle is shown in Fig. 14. Note, however, that in contrast to published opinion in the literature [26,29] the present results allow us to conclude unequivocally that the isobutene generation in self-alkylation is not an isolated dehydrogenation of isobutane, but the hydrogen transfer from isobutane to *n*-butene.

The increasing selectivity to *n*-butane with increasing catalyst lifetime suggests that this route is most pronounced with catalysts fulfilling one criterion for long catalyst life (see Fig. 6). Assuming that the rate of desorption of isobutene is (as a first approximation) independent of the catalyst modifications performed in this study, the production of *n*-butane solely depends on the hydride transfer rate relative to the alkene addition rate. With higher rates of hydride transfer, more *n*-butane will be produced. As

explained above, higher rates of hydride transfer lead to longer catalyst lifetimes, which explains the correlation between lifetime and *n*-butane selectivity. The increase in the 2,2,3-TMP + 2,5-DMH selectivity parallel to the *n*-butane selectivity (see Fig. 7) may also be explained by the increasing hydride transfer activity with increasing lifetime. 2,2,3-Trimethylpentylalkoxide, which is the primary product of the addition of 2-butene to a tertiary butoxide, has less time to isomerize before it receives a hydride and desorbs as 2,2,3-TMP.

The steep increase in 2,2,4-TMP selectivity with the *n*-butane selectivity (also shown in Fig. 7) can be explained by the chemistry isobutene undergoes subsequent to desorption. After isobutene is formed in this cycle, it will be added immediately (alkenes are not detected in reaction mixtures with active catalysts) to another alkoxy group. If this is a tertiary butoxy group, it leads to a 2,2,4-trimethylpentyl. After hydride transfer, 2,2,4-TMP desorbs. Note that this isooctane is thermodynamically favored. It is interesting to note that Li et al., while working with sulfuric acid as alkylation catalyst, found higher 2,2,4-TMP and 2,2,3-TMP selectivities when increasing the strength (concentration) of the acid. The effect was seen with all butene isomers [30]. This observation is in line with our results giving higher 2,2,4-TMP and 2,2,3-TMP selectivities with higher concentrations of strong Brønsted acid sites. It suggests that the same mechanistic principles are operative independent of the chosen acid. Simpson et al. found 2,2,4-TMP to be the main octane isomer when performing isobutane/propene and isobutane/2-pentene alkylation on a H-USY [13]. This allows the conclusion that when using alkenes other than butenes TMPs are mainly produced via the self-alkylation route with minor contributions from cracking products.

However, because in the present experiments even for catalysts with low lifetimes the selectivities to 2,2,4-TMP never fell below 9 wt%, not all 2,2,4-TMP originated from self-alkylation, but also from conventional alkylation followed by isomerization. From our earlier work with H-BEA and from the results of other groups it is known that H-BEA gives very high 2,2,4-TMP selectivities, sometimes as high as 50 wt% [5,31,32]. The *n*-butane selectivity with BEA-based catalysts never exceeded 2 wt%. This led us to conclude that in contrast to what is discussed here, the high selectivity to 2,2,4-TMP in this case is due to the contribution of the conventional alkylation/isomerization route.

2,2,4-TMP has the highest thermodynamic stability among TMPs with relative concentrations at equilibrium amounting to 50 wt%. A high concentration of 2,2,4-TMP produced via the alkylation/isomerization route, therefore, points either to long residence times of the TMPs on the catalyst surface (slower hydride transfer) or to very high isomerization rates.

We speculate at this point that the slower hydride transfer is caused by the higher Si/Al ratio of zeolite BEA compared to La-FAU. Such a conclusion would be in line with findings in cracking experiments, which gave higher hydride transfer rates for zeolites with lower framework Si/Al ratios [33]. Conceptually, a more stable bond between the oxygen of the zeolite and the carbon atom of the alkoxy group should be formed for zeolites with higher a concentration of aluminum in the lattice and a lower acid strength. The fact that it is found experimentally to be easier to remove alkoxy groups with higher stability by hydride transfer strongly suggests that the formation of the new carbon–oxygen bond is of higher importance than the stability of the leaving group.

The H-USY sample of this study gave a moderate lifetime with a correspondingly moderate *n*-butane selectivity, but a significantly higher 2,2,4-TMP selectivity (the circular symbol in Fig. 7). Similar to H-BEA, the higher framework Si/Al ratio (Si/Al $\approx$ 5, as compared to 1.2 in the La-X samples) within the ultrastable FAU may contribute to this deviating behavior. Moreover, it is the only one of the tested samples without La^{3+} ions, the influence of which on the individual reaction rates is not known.

The influence of the pore topology on the selectivities to the individual TMP isomers has been emphasized earlier (see, for example, Yoo et al. [34,35]). Diffusion and electrostatic effects induced by the pore structure certainly play a role and may be responsible in part for the high 2,2,4-TMP selectivity with H-BEA. However, within the range of catalysts examined in this study, 2,2,4-TMP selectivities between 9 and 24 wt% were measured; all samples were of the same pore topology. This clearly evidences that the pore topology is not the dominating factor, but at best one of several.

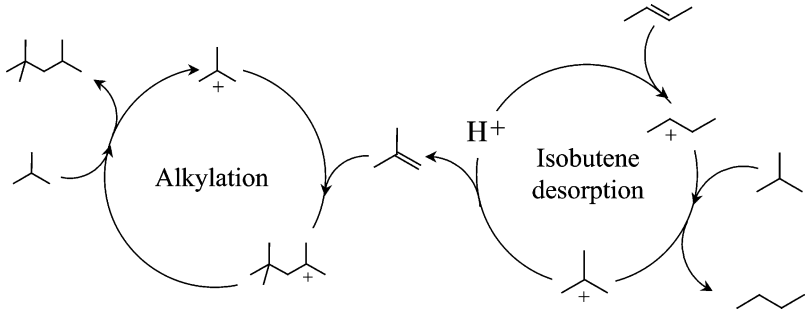

Fig. 14. Self-alkylation cycle, depicting the two steps isobutene desorption and subsequent addition of isobutene to an isobutyl ion to give after hydride transfer 2,2,4-trimethylpentane.

4.4. Influence of the reaction temperature

The influence of the reaction temperature on the alkylation reaction is well documented for liquid acids. Within certain limits, lowering the temperature increases the alkylate quality in terms of selectivity to trimethylpentanes. Corma et al. examined sulfated zirconia as a nonzeolitic solid acid alkylation catalyst in the temperature range −10 to 50 °C. With increasing reaction temperature, the authors found a constantly declining octane and a sharply increasing cracking selectivity. The heavy end selectivity went through a minimum at intermediate temperatures [36].

Zeolites operate at much higher temperatures. For H-BEA, a maximum in the TMP production was found at a reaction temperature of 75 °C, at which also the lifetime was highest. At low temperatures C_{9+} products and at high temperatures cracked products dominated [31]. Tests with H-USY between 40 and 90 °C led to an optimum in lifetime at ca. 65 °C while the TMP selectivity constantly declined with reaction temperature [14].

With the catalysts used in this study, a surprisingly strong dependency of the lifetime and the selectivities on the reaction temperature was observed. The product quality was best (highest C_8 and highest TMP selectivity) at low temperatures, and the lifetime, however, was highest at intermediate temperatures around 75 °C. With increasing temperature, the selectivity to cracking and above 100 °C also to heavy end products increased (see Fig. 10). Cracking via β-scission did not lead to significant formation of propane or propene under the chosen conditions. The smallest cracking product observed was isopentane (isobutane may be formed, but cannot be distinguished from the feed). Therefore, as cracking of a C_8 molecule would lead to the formation of propene or propane, the precursor has to be at least a C_{12} molecule. Consequently, high cracking rates inevitably are coupled with high rates of alkene addition. Within a certain temperature range, however, cracking may actually slow down the buildup of heavy molecules in the catalyst pores.

In contrast to H-BEA and sulfated zirconia noted above, the heavy end selectivity found within the product was low at low reaction temperatures. The much smaller crystals of zeolite H-BEA (primary particles of about 0.1 μm) and the larger pores of sulfated zirconia might allow more heavy molecules to leave the pore system and, thus, give higher heavy end selectivities at low temperatures. Unfortunately, the amount of hydrocarbon retained in the zeolite (between 10 and 20 wt% of the catalyst) was—compared to the total amount of product formed—too low to be accurately accounted for in the mass balance. Typically, the deposits should compose 2–5 wt% of the integral product.

The low lifetimes at low reaction temperatures (see Fig. 8) most likely were a consequence of the severely hindered diffusion of the heavier molecules at low temperatures. The catalysts deactivated by pore blocking. At high reaction temperatures, where diffusion is less problematic, the catalyst also rapidly deactivated. Here, the catalyst deactivates by highly unsaturated compounds, which block the acid site rather than the pore. With increasing reaction temperature, the deposits in deactivated catalysts have been found to be increasingly hydrogen deficient. These compounds are most likely produced through multiple desorption/hydride transfer steps and are strongly bound to the acid sites. Detailed results on the characterization of the deposits used in this study are presented in [37].

The selectivity to dimethylhexanes gradually increases with the reaction temperature. It has been proposed that dimethylhexanes are produced to a major part via cracking of heavier compounds [38]. Thus, when increasing the reaction temperature, alongside the increasing cracking selectivity, more dimethylhexanes are also produced. The decreasing production of trimethylpentanes is a consequence of the higher rates of the secondary reactions, cracking and alkene addition. Before the TMP precursors can desorb via hydride transfer they are alkylated again. The selectivities to *n*-butane, 2,2,4-TMP, and 2,2,3-TMP + 2,5-DMH pass through a maximum, indicating that the self alkylation activity has a temperature optimum around 75 °C. This suggests that the conditions favoring self alkylation activity also favor a long catalyst lifetime. This has been confirmed by using smaller alkenes than butene. By doing so, the TMPs produced should originate mainly from self alkylation. With propene and ethene on H-BEA, Nivarthy et al. [39] found a maximum in the octane selectivity also at ca. 75 °C, indicating that a facilitation of the difficult step, the hydride transfer, is crucial for successful operation.

4.5. Influence of the olefin space velocity

The constant productivity of the catalysts with varying OSV is of high importance for the practical application of the catalyst. It suggests that isomerization and hydride transfer are fast compared to the alkene addition under the practical conditions investigated, i.e., that the alkene addition is rate limiting. There may be, however, a critical OSV, at which insufficient rates of hydride transfer will lead to the preferential formation of higher hydrocarbons via multiple alkylation. The decreasing selectivities to *n*-butane, 2,2,4-TMP, and 2,2,3-TMP + 2,5-DMH with increasing OSV (i.e., with decreasing $(\mathrm{OSV})^{-1}$, see Fig. 10c) suggest that the fraction of isobutene desorbing and acting as alkylating agent has decreased, however. With the higher throughput of butenes the probability that the butoxy groups can decompose before being alkylated is reduced, decreasing in this way the importance of the self alkylation route.

4.6. The nominal butene feed rate per active site controls the overall selectivity

The results of the experiments with added deactivated catalyst (shown in Figs. 11 and 12) connect the findings with catalysts of different acid site distributions and the findings

of the OSV study. The individual acid sites in the fresh catalyst fraction experience a higher OSV and give accordingly changing C_8 selectivities. The deactivated catalyst fraction, however, is not completely inert, but produces a low-quality alkylate most likely with a high fraction of octenes. The unsaturated products will react with alkoxy groups and contribute to the increased heavy end formation. Catalysts with an intrinsically high concentration of weak Brønsted acid sites behave similarly. In such a catalyst, the (small) fraction of strong Brønsted acid sites experiences a relatively higher OSV than in a superior catalyst with a high fraction of strong Brønsted acid sites. Thus, the selectivities measured with catalysts of different lifetimes (see Fig. 6) resemble the selectivities measured with one sample under changing OSV. Figs. 6, 10, and 12 all exemplify the behavior of alkylation catalysts under changing severity of operation per individual active site. In all of these figures the nominal butene feed rate per site decreases along the *X* axis. With decreasing nominal feed rate the relative importance of hydride transfer increases, leading to the observed changes in the selectivities, i.e., increasing selectivities to *n*-butane, and 2,2,3-TMP, 2,2,4-TMP and decreasing selectivities to heavy end products.

5. Conclusions

The avoidance of structural damage occurring during the modification procedure is the key factor for suitable faujasitic alkylation catalysts. It ensures a high B/L ratio, which minimizes the alkene concentration close to the Brønsted acid sites. In this way, hydride transfer will be favored over alkene addition. Maximizing the concentration of strong Brønsted acid sites thus reduces oligomerization significantly. Two mechanistic pathways lead to the formation of heavy end products and ultimately to catalyst deactivation, i.e., multiple alkylation on the stronger sites and oligomerization on the weaker. Both routes can be minimized through optimizing ion exchange and calcination on the one hand and reaction conditions on the other.

Self-alkylation activity is linked to the acid strength of the catalyst. It is, therefore, most likely an indicator rather than a prerequisite of a suitable catalyst. Brønsted acid sites with a strength required for alkylation also allow self-alkylation. Unfortunately, the higher production of *n*-butane lowers somewhat the octane yield. In this respect, the behavior of faujasitic catalysts resembles that of hydrofluoric acid.

Alkylation is a very temperature-sensitive reaction. The optimum in lifetime is not necessarily the optimum in alkylate quality. A compromise has to be found between a sufficiently fast diffusion of bulky products and acceptable ratios of hydride transfer and alkene addition rates. Cracking might be of help to slow down the buildup of the coke precursors.

Within the range tested here, the integral yields did not change significantly with the OSV. The selectivities, however, strongly depend on the nominal butene feed rate per strong Brønsted acid site. These results show that the best of the tested materials are robust alkylation catalysts and can be used under severe conditions without major drawbacks in alkylate quality.

Acknowledgments

The authors thank Marcus Breuninger of Süd-Chemie AG for providing several of the examined samples. Financial support from Süd-Chemie AG is gratefully acknowledged.

References

[1] J. Stell, Oil Gas J. 99 (2001) 74.
[2] Anonymous, Oil Gas J. 98 (2000).
[3] J. Weitkamp, Y. Traa, in: G. Ertl, H. Knözinger, J. Weitkamp (Eds.), Handbook of Heterogeneous Catalysis, vol. 4, VCH, Weinheim, 1997, p. 2039.
[4] A. Corma, A. Martinez, Catal. Rev.-Sci. Eng. 35 (1993) 483.
[5] G.S. Nivarthy, K. Seshan, J.A. Lercher, Micropor. Mesopor. Mater. 22 (1998) 379.
[6] G.S. Nivarthy, K. Seshan, J.A. Lercher, Stud. Surf. Sci. Catal. 126 (1999) 465.
[7] M. Stöcker, H. Mostad, A. Karlsson, H. Junggreen, B. Hustad, Catal. Lett. 40 (1996) 51.
[8] F.A. Diaz-Mendoza, L. Pernett-Bolano, N. Cardona-Martinez, Thermochim. Acta 312 (1998) 47.
[9] A. Feller, I. Zuazo, A. Guzman, J.O. Barth, J.A. Lercher, J. Catal. 216 (2003) 313.
[10] A. Corma, A. Martinez, P.A. Arroyo, J.L.F. Monteiro, E.F. Sousa-Aguiar, Appl. Catal. A 142 (1996) 139.
[11] C. Flego, I. Kiricsi, W.O. Parker Jr., M.G. Clerici, Appl. Catal. A 124 (1995) 107.
[12] K.P. de Jong, C.M.A.M. Mesters, D.G.R. Peferoen, P.T.M. van Brugge, C. de Groot, Chem. Eng. Sci. 51 (1996) 2053.
[13] M.F. Simpson, J. Wei, S. Sundaresan, Ind. Eng. Chem. Res. 35 (1996) 3861.
[14] R. Taylor, D.E. Sherwood Jr., Appl. Catal. A 155 (1997) 195.
[15] R.B. Borade, A. Clearfield, J. Phys. Chem. 96 (1992) 6729.
[16] J.F. Lindsley, U.S. patent 4,125,591, 1978.
[17] B.H. Wouters, T.H. Chen, P.J. Grobet, in: Proceedings of the 13th International Zeolite Conference, Montpellier, 2001, p. 344.
[18] M. Weihe, M. Hunger, M. Breuninger, H.G. Karge, J. Weitkamp, J. Catal. 198 (2001) 256.
[19] J.A. van Bokhoven, A.L. Roest, D.C. Koningsberger, J.T. Miller, G.H. Nachtegaal, A.P.M. Kentgens, J. Phys. Chem. B 104 (2000) 6743.
[20] G.H. Kuehl, H.K.C. Timken, Micropor. Mesopor. Mater. 35–36 (2000) 521.
[21] K. Gaare, D. Akporiaye, J. Phys. Chem. B 101 (1997) 48.
[22] L. Schmerling, J. Am. Chem. Soc. 67 (1945) 1778.
[23] L. Schmerling, J. Am. Chem. Soc. 68 (1946) 275.
[24] H.B. Mostad, M. Stöcker, A. Karlsson, T. Rørvik, Appl. Catal. A 144 (1996) 305.
[25] A. Corma, A. Martinez, C. Martinez, J. Catal. 146 (1994) 185.
[26] F. Cardona, N.S. Gnep, M. Guisnet, G. Szabo, P. Nascimento, Appl. Catal. A 128 (1995) 243.
[27] J. Pater, F. Cardona, C. Canaff, N.S. Gnep, G. Szabo, M. Guisnet, Ind. Eng. Chem. Res. 38 (1999) 3822.
[28] J.E. Hofmann, J. Org. Chem. 29 (1964) 1497.

[29] M. Guisnet, N.S. Gnep, Appl. Catal. A 146 (1996) 33.
[30] K.W. Li, R.E. Eckert, L.F. Albright, Ind. Eng. Chem. Process Des. Dev. 9 (1970) 441.
[31] G.S. Nivarthy, Y. He, K. Seshan, J.A. Lercher, J. Catal. 176 (1998) 192.
[32] A. Corma, V. Gomez, A. Martinez, Appl. Catal. A 119 (1994) 83.
[33] K.A. Cumming, B.W. Wojciechowski, Catal. Rev.-Sci. Eng. 38 (1996) 101.
[34] K. Yoo, E.C. Burckle, P.G. Smirniotis, Catal. Lett. 74 (2001) 85.
[35] K. Yoo, E.C. Burckle, P.G. Smirniotis, J. Catal. 211 (2002) 6.
[36] A. Corma, A. Martinez, C. Martinez, J. Catal. 149 (1994) 52.
[37] A. Feller, J.O. Barth, A. Guzman, I. Zuazo, J.A. Lercher, J. Catal. 220 (2003) 192.
[38] L. Lee, P. Harriott, Ind. Eng. Chem. Process Des. Dev. 16 (1977) 282.
[39] G.S. Nivarthy, A. Feller, K. Seshan, J.A. Lercher, Micropor. Mesopor. Mater. 35–36 (2000) 75.